Excited-State Distortions in Bis[hydrotris(3,5-dimethyl-1-pyrazolyl)borato]copper(II) Determined from Resonance Raman Intensities and a Normal Coordinate Analysis

Jeffrey L. Wootton and Jeffrey I. Zink*

Department of Chemistry and Biochemistry, University of California, Los Angeles, Los Angeles, California 90095

Guillermo Díaz Fleming*

Universidad de Playa Ancha, Facultad de Ciencias, Casilla 34-V, Valparaíso, Chile

Marcelo Campos Vallette

Universidad de Chile, Facultad de Ciencias, Casilla 653, Santiago, Chile

Received August 19, 1996[⊗]

Resonance Raman spectra, a normal coordinate analysis, and calculation of excited-state bond lengths and angles of bis[hydrotris(3,5-dimethyl-1-pyrazolyl)borato]copper(II) are reported. Raman spectra are obtained in resonance with a ligand field state and the lowest ligand-to-metal charge transfer (LMCT) excited state. A normal coordinate analysis is carried out using Raman and IR frequencies and resonance Raman intensities to assist in the assignment of the symmetric modes. Potential energy distributions (PED) and force constants are reported. The individual bond length changes are calculated by using the resonance Raman intensities and the PED. Bond length and angle changes throughout the entire three-dimensional skeleton are reported. The signs of the bond length changes in the pyrazolyl borate ring are interpreted in conjunction with the results of a molecular orbital calculation. The N−N bond length decreases by 0.02 Å, the C═N bond lengths increase by 0.05 and 0.08 Å, the Cu−N bond increases by 0.10 Å and the N−B−N angle decreases by 2° in the LMCT excited state.

Introduction

The coordination chemistry of poly(pyrazol-1-yl)borate ligands, discovered more than 25 years ago, continues to attract interest.[1−4] The interest in the tripodal tris(pyrazolyl)borates stems from the fact that regiospecific substituents in the pyrazole rings allow control of steric factors. This has enabled the synthesis and structure determination of complexes capable of both activation of small molecules like dinitrogen and dioxygen, and of catalytic activity.[5] The copper complexes with these ligands are also of interest from the bioinorganic point of view because the rigid N_3 ligand coordination mimics the spectroscopic characteristics of "blue" copper proteins.[6]

Resonance Raman intensities have been used to determine excited state distortions for a number of molecules.[7−18] Specifically, excited state distortions resulting from charge transfer and electron transfer excited states of inorganic and organic molecules have been of particular interest.[10] Recently absorption, fluorescence, and resonance Raman spectroscopies were used to measure the excited-state distortions in plastocyanin, which is involved in electron transport for plant photosynthesis.[11]

Compared to the enormous number of synthetic and structural studies of pyrazolyl borato complexes, few vibrational studies have been performed. One work[19] deals with low-frequency IR spectral assignments of several poly(pyrazolyl)borate complexes, and recently a complete vibrational study of hydrotris(pyrazolyl)borato complexes of rhenium(I) tricarbonyl[20] was reported.

In this paper we report the resonance Raman intensities, a normal coordinate analysis, and the calculation of the excited state bond length and angle changes in bis[hydrotris(3,5-dimethyl-1-pyrazolyl)borato]copper(II), $Cu(Tp^*)_2$. Resonance Raman spectroscopy plays a multifaceted role in this study. The intensities observed in the resonance Raman spectra are related to the excited state distortions. The distortions are used not only to assist in the assignments of the symmetric normal modes, but also to calculate the excited state distortions. The normal

[⊗] Abstract published in *Advance ACS Abstracts,* February 1, 1997.

(1) Trofimenko, S. *Chem. Rev.* **1993**, *34*, 443 and references cited therein.
(2) Trofimenko, S. *Prog. Inorg. Chem.* **1986**, *34*, 115.
(3) Kitajima, N.; Moro-oka, Y.; Uchida, A.; Sasada, Y.; Ohashi, Y. *Acta Crystallogr.* **1988**, *C44*, 1876.
(4) Ha, E. H.; Ho, R. Y.; Kisiel, J. F.; Valentine, J. S. *Inorg. Chem.* **1995**, *34*, 2265.
(5) Han, R.; Parkin, G. *J. Am. Chem. Soc.* **1990**, *112*, 3662.
(6) Kitajima, N.; Fujisawa, K.; Moro-oka, Y. *J. Am. Chem. Soc.* **1990**, *112*, 3210.
(7) Tannor, D. J.; Sundberg, R. L.; Heller, E. J. *J. Phys. Chem.* **1982**, *86*, 1822.
(8) Tang, J.; Albrecht, A. C. *Raman Spectoscopy*; Szynanski, H., Ed.; Plenum Press: New York, 1970; Vol. 2, p 33.
(9) Zink, J. I.; Shin, K. S. K. *Adv. Photochem.* **1991**, *16*, 119.
(10) Myers, A. B. *Chem. Rev.* **1996**, *96*, 911.
(11) Fraga, E.; Webb, M. A.; Loppnow, G. R. *J. Phys. Chem.* **1996**, *100*, 3278.
(12) Wright, P. G.; Stein, P.; Burke, J. M.; Spiro, T. G. *J. Am. Chem. Soc.* **1979**, *101*, 3531.
(13) Rush, T., III; Kumble, R.; Mukherjee, A.; Blackwood, M. E., Jr.; Spiro, T. G. *J. Phys. Chem.* **1996**, *100*, 12076.
(14) Peticolas, W. L.; Strommen, D. P.; Lakshminarayanan, V. *J. Chem. Phys.* **1980**, *73*, 4185.
(15) Peticolas, W. L.; Rush, T., III. *J. Comput. Chem.* **1995**, *16*, 1261.
(16) Zink, J. I. *Coord. Chem. Rev.* **1985**, *64*, 93.
(17) Tutt, L.; Zink, J. I. *J. Am. Chem. Soc.* **1986**, *108*, 5830.
(18) Zink, J. I.; Reber, C. *Coord. Chem. Rev.* **1991**, *111*, 1.
(19) Hutchinson, B.; Hoffbauer, M.; Takemoto, J. *Spectrochim. Acta* **1976**, *32A*, 1785.
(20) Díaz, G. F.; Campos, M. V.; Klahn, A. H. O. *Vib. Spectrosc.* **1995**, *9*, 257.

S0020-1669(96)01006-3 CCC: $14.00

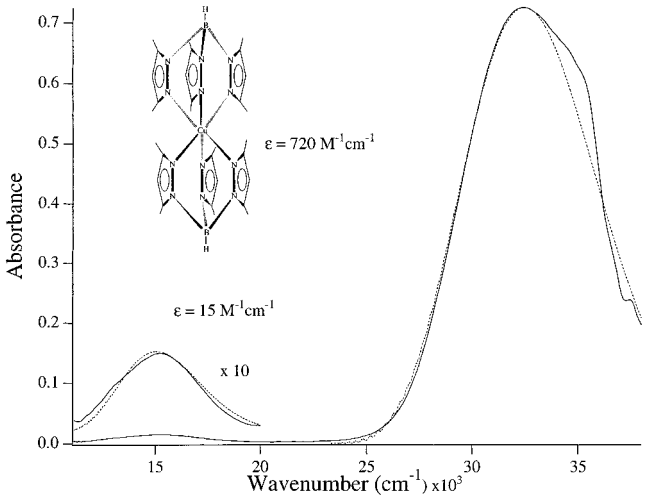

Figure 1. Absorption spectrum of $Cu(Tp^*)_2$ in CH_2Cl_2. The dashed lines are the absorption bands calculated from the resonance Raman determined distortions given in Table 4.

coordinate analysis is necessary to calculate the bond length and angle changes because vibrations of the entire three-dimensional skeleton are strongly mixed. Our results give a picture of the molecule after electron transfer from the Tp* ligand to the copper metal.

Experimental Section

Materials. The hydrotris(pyrazolyl)borato ligand salt, KTp*, was purchased from Aldrich and used as received. The complex $Cu(Tp^*)_2$ was prepared according to the literature procedure.[3]

Spectroscopy. The absorption spectrum of a 1×10^{-3} M solution of $Cu(Tp^*)_2$ in CH_2Cl_2 was recorded with a Shimatsu-UV 260 spectrophotometer and is shown in Figure 1.

FT-IR spectra of ligands and complexes as KBr pellets were recorded in the spectral domain of 4000−400 cm^{-1} using a Perkin-Elmer Series 2000 instrument. FT-IR spectra of compounds as polyethylene pellets were registered between 450 and 120 cm^{-1} by using a Bruker 66 V spectrometer. Spectra were scanned with a resolution of 2 cm^{-1}. Two hundred scans were accumulated for both the mid- and far-IR measurements.

Resonance Raman and Raman spectra were recorded using argon ion (363.8, 457.9, and 514.5 nm) or krypton ion (647.1 nm) excitation at room temperature. The laser beam was focused on the samples with a 150 nm focal length lens. The scattered light was collected and passed through a triple monochromator (Instruments SA, Inc., Models DHR320 and HR640) and detected by a charge coupled device, CCD (Princeton Research). The CCD was calibrated with the emission lines of a neon bulb and with the Raman spectra of liquid toluene, dioxane, DMF, and solid Bi_2O_3. The resulting experimental frequencies have at most a ± 2 cm^{-1} uncertainty. The resonance Raman intensities were measured by taking the integrated area of each peak.

Results

Spectroscopy. The absorption spectrum of a 1×10^{-3} M solution of $Cu(Tp^*)_2$ in CH_2Cl_2 between 10 000 and 40 000 cm^{-1} is shown in Figure 1 (solid lines). Two absorption bands are observed with maxima at 15 900 and 32 900 cm^{-1} with extinction coefficients of 15 M^{-1} cm^{-1} and 720 M^{-1} cm^{-1} respectively. The full width at half maximum of the 15,900 cm^{-1} band is 4500 cm^{-1} while the band at 32 ,900 cm^{-1} has a full width at half-maximum of 7400 cm^{-1}. The calculated absorption spectra (*vide infra*) are also shown in the figure.

The observed FT-IR and Raman frequencies are given in Table 1 along with the assignments based on the normal coordinate analysis and the resonance Raman intensity data. The force constants used in the normal coordinate calculations are given in Table 2. The calculated frequencies and the potential energy distribution are given in Table 3.

Table 1. Observed FT-IR and Raman Frequencies (cm^{-1}) for $Cu(Tp^*)_2$

IR	Raman	assignment
	3134	
3109 w	3117	
3100 w		ν(CH)
2924 m	2933	
2861 m		$\nu(CH_3)$
2506 s	2506	ν(BH)
	1549	
1540 s	1542	ν(CC)
1445 s	1452	$\delta(CH_3)$ asym
1415 s		ν(CN)
	1385	$\delta(CH_3)$ sym
1381 s	1376	ν(CC)
1364 s		
	1348	δ(BH)
	1213	
1203 s	1202	ν(NN)
1187 s		
		ν(NN)
1142 w	1143	
	1129	ring breathing
1073 sh	1069	δ(CH)
1065 s	1058	$\nu(C-CH_3)$
1035 ms	1037	
989 m	980	
936 s		δ(CH) oop
865 w	866	$\rho(CH_3)$
845 mbr	850	
807 s	804	
	774	$\nu(C-CH_3)$
768 mbr	752	
700 m	700	
693 m	690	ν(BN)
	660	
647 s	648	ring def
	643	
	598	
	590	ring twist
580 w		
469 ms	463	ring def
454 mw	454	$\delta(C-CH_3)$
400 sh		
394 m	390	δ(NBN)
	382	
358 mbr	361	ν(CuN)
	325	
315 m		
275 mbr		
256 m	253	δ(NBN)
237 m	236	δ(NCuN)
161 mw		

The resonance Raman spectra of solid $Cu(Tp^*)_2$ at 298 K with 647.1 and 363.8 nm excitation are shown in Figure 2. The relative resonance Raman intensities with 647.1, 363.8, and 457.9 nm excitation along with their corresponding distortions are given in Table 4.

Discussion

1. Normal Coordinate Analysis and Vibrational Assignments. In Table 1 are presented the IR and Raman data obtained for $Cu(Tp^*)_2$. In this table we have also included the assignments. The bands were assigned based on three lines of reasoning. First, bands in a given region are frequently characteristic of vibrations from a given part of the molecule,

Table 2. Valence Force Constants for $Cu(Tp^*)_2$[a]

Diagonal Force Constants

no.	stretch	force const (mdyn/Å)	no.	stretch	force const (mdyn/Å)
1	CuN	0.95	6	$(CC)_b$	6.05
2	NN	5.85	7	$(NC)_b$	6.20
3	BN	4.22	8	$(C\text{-}Me)_a$	4.00
4	$(NC)_a$	6.10	9	$(C\text{-}Me)_b$	4.03
5	$(CC)_a$	6.00	10	CH	5.0

no.	bend	force const (mdyn Å/rad^2)	no.	bend	force const (mdyn Å/rad^2)
1	NCuN	0.25	5	$(NCMe)_a$	0.32
2	NBN	1.18	6	$(NCMe)_b$	0.36
3	$(NCC)_a$	1.66	7	CCH	0.68
4	$(NCC)_b$	1.67			

no.	oop bend	force const (mdyn Å/rad^2)	no.	oop bend	force const (mdyn Å/rad^2)
1	HCCC	0.37	3	$(MeCNC)_b$	0.21
2	$(MeCNC)_a$	0.20			

no.	torsion	force const (mdyn Å/rad^2)
1	NCCC	0.64

Interaction Force Constants[c]

no.	force const	no.	force const	no.	force const	no.	force const
Stretch−Stretch Interactions (mdyn/Å)							
1−1	0.16	5−6	0.64	4−5	0.62	6−7	0.62
3−4	0.45	2−4	0.50	2−7	0.50	3−3	0.20
1−2	0.10	1−7	0.08	2−3	0.38	3−5	0.09
2−5	0.09	2−6	0.08	4−7	0.08	4−6	0.09
5−7	0.12	1−3	−0.05				
Stretch−Bend Interactions (mdyn/Rad)							
3−3	0.12	5−3	0.12	6−4	0.12	3−2	0.25
7−4	0.12	8−3	0.05	9−4	0.05	4−5	0.04
5−5	-0.07	6−6	−0.07	5−7	0.04	4−7	0.07
4−3	0.12	7−6	0.05				
Bend−Bend Interactions (mdyn Å/rad^2)							
2−3	0.15	2−2	-0.15	3−4	0.08	3−5	0.05
4−6	0.05						

Bend−oop Bend Interactions (mdyn Å/rad^2)

no.	force const	no.	force const
7−2	0.05	7−3	0.15

[a] The "a" label denotes the internal coordinates of the part of the pyrazolyl ring near the boron. [b] The "b" label denotes the internal coordinates of the part of the pyrazolyl ring near the copper. [c] The numbers refer to the corresponding diagonal terms.

e.g. pyrazolyl ring stretching modes in the 980−1600 cm^{-1} region. Second, resonance Raman intensities assist in identifying the totally symmetric modes. Third, the normal coordinate analysis that uses force constants transferred from analogous systems provides detailed insight. These three aspects are discussed in detail below.

In the region 3200−2850 cm^{-1} we find weak and medium absorptions involving ν(C−H) and ν(C−H_3). The medium sharp band observed in the IR spectrum at about 2500 cm^{-1} is characteristic of the B−H stretching mode. This band is weak in the Raman spectrum.

Bands in the range 1600−980 cm^{-1} can be attributed to pyrazolyl ring stretching modes according to a vibrational study of pyrazole by Durig et al.[21] In this region we also expect to find frequencies involving δ(CH), which have been reported at about 1300−1000 cm^{-1} in complexes with conjugated ligand systems such as bipyridine[22] and porphyrin.[23] This type of vibration also participates in higher frequency modes.

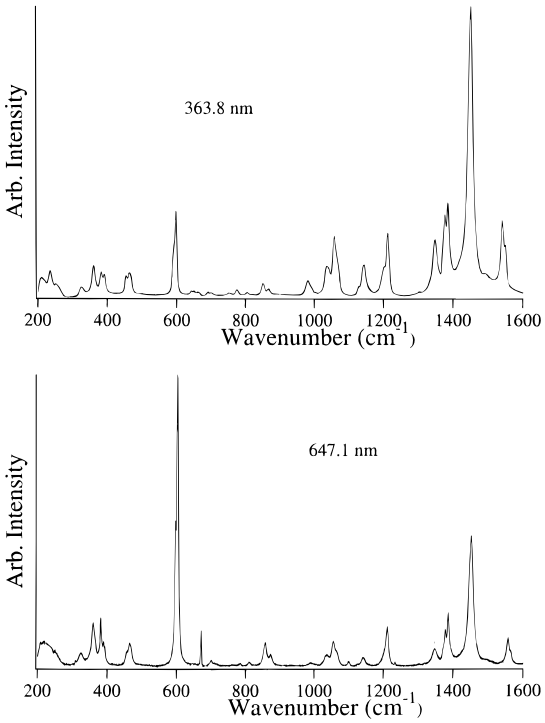

Figure 2. Resonance Raman spectra of $Cu(Tp^*)_2$ from 200 to 1600 cm^{-1} with 363.8 nm excitation which is in resonance with the LMCT absorption band (top) and 647.1 nm excitation which is in resonance with the ligand field absorption band (bottom).

In the region 1500−700 cm^{-1}, broad bands, shoulders, and new bands that are absent in the non-methylated $Cu(Tp)_2$ observed near 1450 cm^{-1} [$\delta(CH_3)$ as], 1380 cm^{-1} [$\delta(CH_3)$ sym], and 800 cm^{-1} [$\rho(CH_3)$] denote the presence of the methyl groups.[24] Further, ν(C−CH_3) has been reported in the range 1100−900 cm^{-1} in several complexes with methyl-substituted ligands.[25−28]

Between 1000 and 800 cm^{-1} out-of-plane δ(CH) have been calculated in the work by Li et al.[22] Bands in the range 800−600 cm^{-1} can be assigned to pyrazolyl bending or twisting vibrations following Durig et al.[21] In this range we should also expect the presence of the B−N stretch vibrations. Taylor and Cluff[29] found that the boron−nitrogen dative bond in amine−borane complexes gives rise to a band between 800 and 650 cm^{-1}.

Below 600 cm^{-1}, one can expect to find those normal modes corresponding to ring torsions, as well as bending movements (in-plane and out-of-plane) of the CH_3 groups in the region around 400 cm^{-1}.[27] Between 400 and 200 cm^{-1} bands have

(21) Durig, J. R.; Bergana, M. M.; Zunic, W. M. *J. Raman Spectroc.* **1992**, *23*, 357.
(22) Mallick, P. K.; Danzer, G. D.; Strommen, D. P.; Kincaid, J. R. *J. Phys. Chem.* **1988**, *92*, 5628.
(23) Li, X.; Czernuszewicz, R. S.; Kincaid, J. R.; Su, Y. O.; Spiro, T. G. *J. Phys. Chem.* **1990**, *94*, 31.
(24) Colthup, N. B.; Daly, L. H.; Wiberly, S. E. *Introduction to IR and Raman Spectroscopy*, 3rd Ed.; Academic Press: New York, 1990; pp 223−233.
(25) Siimann, O.; Fresco, J. *J. Chem. Phys.* **1971**, *54*, 740.
(26) Barraclough, C. G.; Martin, R. L. *Aust. J. Chem.* **1969**, *22*, 891.
(27) Heath, G. A.; Martin, R. L. *Aust. J. Chem.* **1970**, *23*, 1721.
(28) Siimann, O.; Fresco, J. *Inorg. Chem.* **1971**, *10*, 297.
(29) Taylor, R. C.; Cluff, C. L. *Nature* **1958**, *182*, 390.

Table 3. Calculated Frequencies and Potential Energy Distrubtion (PED)[a−c]

A_1 Modes

obsd res enhanced modes	calcd	potential energy distribution
1542	1546	20% $\nu(CC)_b$ + 16% $\nu(CC)_a$ + 17% $\nu(NC)_a$ + 14% $\delta(NCC)_a$ +15% $\delta(CCH)$
1452	1451	17% $\nu(NC)_a$ + 18% $\nu(NC)_b$ + 16% $\delta(NCC)_b$ + 16% $\nu(NN)$ + 10% $\nu(CC)_a$
1385	1380	43% $\nu(CC)_b$ + 35% $\nu(NC)_b$ + 8% $\nu(CC)_a$ + 6% $\nu(NC)_a$
1348	1351	40% $\nu(CC)_a$ + 29% $\nu(NC)_a$ + 14% $\nu(NC)_b$ + 10% $\nu(CMe)_b$
1213	1218	59% $\nu(NN)$ + 20% $\nu(BN)$ + 9% $\nu(NC)_b$ + 8% $\nu(NC)_a$
1069	1065	60% $\delta(CCH)$ + 14% $\nu(CMe)_b$ + 8% $\nu(NC)_b$ + 5% $\delta(NCC)_b$
980	985	73% $\gamma(HCCC)$ + 19% $\tau(NCCC)$
866	929	35% $\nu(CMe)_a$ + 17% $\nu(BN)$ + 15% $\nu(CC)_a$ + 10% $\delta(NCC)_a$ + 9% $\nu(NN)$
804	811	26% $\nu(CMe)_b$ + 24% $\nu(CC)_b$ + 13% $\delta(CCH)$ + 12% $\nu(NC)_b$ + 9% $\nu(BN)$
690	688	32% $\nu(BN)$ + 11% $\delta(NBN)$ + 12% $\nu(NC)_a$ + 12% $\delta(NCC)_b$ + 21% $\nu(CMe)_a$ + 10% $\nu(CMe)_b$
590	571	49% $\tau(NCCC)$ + 26% $\gamma(HCCC)$ + 19% $\gamma(MeCNC)_a$ + 6% $\gamma(MeCNC)_b$
454	446	34% $\delta(NCC)_b$ + 20% $\delta(NCC)_a$ + 8% $\nu(NN)$ + 17% $\nu(CMe)_b$ + 13% $\nu(CMe)_a$
382	386	77% $\gamma(MeCNC)_b$ + 22% $\gamma(MeCNC)_a$
361	366	37% $\delta(NBN)$ + 26% $\nu(CuN)$ + 37% $\delta(NCC)_a$
325	296	52% $\delta(NBN)$ + 19% $\nu(CuN)$ + 14% $\delta(NCMe)_a$
253	248	29% $\delta(NCMe)_a$ + 50% $\delta(NCMe)_b$ + 15% $\nu(CuN)$
	158	29% $\delta(NCuN)$ + 16% $\nu(CuN)$ + 11% $\delta(NCC)_b$ + 19% $\delta(NCMe)b$ + 10% $\delta(NCMe)_a$

E Modes

calcd	potential energy distribution
1539	21% $\nu(CC)_b$ + 17% $\nu(CC)_a$ + 15% $\nu(NC)_a$ + 15% $\nu(CMe)_?$ +14% $\delta(NCC)_a$ + 16% $\delta(CCH)$
1449	21% $\nu(NC)_a$ + 17% $\nu(NC)_b$ + 15% $\delta(NCC)_b$ + 15% $\nu(CMe)_b$ + 9% $\nu(CC)_a$ + 7% $\nu(CC)_b$ + 15% $\nu(NN)$
1381	40% $\nu(NC)_b$ + 31% $\nu(CC)_b$ + 15% $\nu(NC)_a$ + 10% $\nu(BN)$ + 6% $\nu(CMe)_a$
1366	37% $\nu(CC)_a$ + 14% $\nu(CC)_a$ + 17% $\nu(NC)_a$ + 12% $\nu(CC)_b$ + 5% $\nu(CMe)_a$ + 9% $\nu(CMe)_b$
1265	37% $\nu(NN)$ + 34% $\nu(BN)$ + 18% $\nu(NC)_b$ + 7% $\nu(NC)_a$
1076	41% $\delta(CCH)$ + 19% $\nu(NN)$ + 12% $\nu(CMe)_b$ + 10% $\nu(CC)_a$ + 8% $\nu(BN)$
1026	23% $\delta(CCH)$ + 16% $\nu(BN)$ + 13% $\nu(CMe)_a$ + 5% $\nu(NC)_b$ + 8% $\nu(NC)_a$ + 16% $\nu(NN)$
986	72% $\gamma(HCCC)$ + 19% $\tau(NCCC)$
852	20% $\nu(CMe)_a$ + 6% $\nu(CMe)_b$ + 10% $\delta(NCC)_b$ + 7% $\delta(NCC)_a$ + 7% $\nu(NC)_b$ + 10% $\nu(NC)_b$ + 6% $\delta(NBN)$ + 4% $\nu(BN)$
770	29% $\nu(CMe)_b$ + 20% $\nu(CMe)_a$ + 13% $\nu(CC)_b$ + 7% $\nu(NC)_b$ + 7% $\nu(CC)_a$ + 7% $\nu(NC)_a$ + 6% $\delta(NBN)$ + 8% $\delta(CCH)$
593	41% $\tau(NCCC)$ + 24% $\gamma(HCCC)$ + 15% $\gamma(MeCNC)_b$ + 10% $\delta(NBN)$
456	33% $\delta(NCC)_b$ + 30% $\delta(NBN)$ + 10% $\nu(CMe)_b$ + 8% $\gamma(MeCNC)_b$
389	67% $\gamma(MeCNC)_b$ + 17% $\gamma(MeCNC)_a$
329	26% $\delta(NBN)$ + 13% $\nu(CuN)$ + 9% $\nu(BN)$ + 8% $\delta(NCC)_a$ + 7% $\delta(NCC)_b$ +9% $\delta(NCMe)_a$ + 11% $\gamma(MeCNC)_a$
239	54% $\delta(NCMe)_b$ + 26% $\delta(NCMe)_a$ + 16% $\nu(CuN)$
166	33% $\delta(NCuN)$ + 6% $\nu(CuN)$ + 11% $\delta(NCC)_a$ + 18% $\delta(NCMe)_a$

[a] The "a" label denotes the internal coordinates of the part of the pyrazolyl ring near the boron. [b] The "b" label denotes the internal coordinates of the part of the pyrazolyl ring near the copper. [c] ν = stretching, δ = bending, γ = out-of-plane bending, τ = torsion.

been reported involving ν(Cu−N)[20] and δ(NBN).[19] The δ(NCuN) vibration should be located below 200 cm^{-1}.

The general spectral pattern is consistent with effective C_{3v} symmetry. An appropriate model for the normal coordinate calculations involves a single Tp* ligand, e.g. the top half of the molecule drawn in Figure 1, because coupling between Tp* ligands is expected to be small. The methyl groups were treated as 15 amu point masses because it is simpler and because they do not contribute directly to the resonance Raman spectra.

The normal coordinate analysis was performed by utilizing the Wilson GF matrix method[30] and using the well-documented Schachtschneider programs.[31] The geometrical parameters used in this calculation were taken from the X-ray crystal structure of $Cu(Tp^*)_2$.[3] The bond lengths were slightly modified to match a C_{3v} symmetry. The internal coordinates obtained from the model were used to form the symmetry coordinates transforming under the A_1 and E irreducible representations of the C_{3v} point group.

A valence force field with 21 diagonal force constants was used. For the sake of completeness, 39 nondiagonal terms representing the most relevant interactions were considered.

Values for f_{BN} and f_{NN} and related angles were transferred from those used for $(Tp^*)Re(CO)_3$.[20] Force constants for the pyrazolyl groups were taken from the work by Durig for pyrazole.[21] The Cu−N force constant was estimated from current values given for copper(II) polyamine complexes.[32,33] Force constants for stretching and bending of the $C-CH_3$ moiety were obtained from different methyl substituted molecules.[34−37]

The stretch-bend interaction force constants that involve a common bond are always included in our calculation. One of the most commonly employed strategies to reduce the number of off-diagonal elements is to neglect stretch−stretch interaction constants that do not include a common atom. However, it has been pointed out that in the case of conjugated systems, this kind of nondiagonal force constant is important.[38] This concept has been convincingly supported by Califano et al. in their studies of the vibrational spectra of polycyclic aromatic hydrocarbons.[39] In addition, the interaction of the hydrogen wagging motion with the stretching coordinate that shares a common carbon atom and the stretch wagging interaction with a bond in common are included in our calculation. We find that the results are unchanged when the sign relationship

(30) Wilson, E. B.; Decius, J. C.; Cross, P. C. *Molecular Vibrations*; McGraw-Hill: New York, 1955.
(31) Schachtschneider, J. H. Technical Reports No. 231-64 and 51-65, Shell Development Co.: Emeryville, CA, 1962.
(32) Díaz, G.; Diez, S.; Lopez, L.; Muñoz, H.; Pessoa, H.; Campos, M. *Vib. Spectrosc.* **1992**, *3*, 315.
(33) Díaz, G.; Bustos, C.; Shepherd, R. E. *Spectrochim. Acta* **1987**, *43A*, 1141.
(34) Crowder, G. A.; Tian, W. *Spectrosc. Lett.* **1994**, *27*, 967.
(35) Crowder, G. A.; Singh, V. K. B. *Spectrosc. Lett.* **1995**, *28*, 1137.
(36) Gladkov, L. L.; Solovyov, K. N. *Spectrochim. Acta* **1985**, *41A*, 1443.
(37) Piffat, C.; Melamed, D.; Spiro, T. G. *J. Phys. Chem.* **1993**, *97*, 7441.
(38) Scherer, J. R.; Overend, J. *Spectrochim. Acta* **1961**, *17*, 719.
(39) Neto, N.; Scrocco, M.; Califano, S. *Spectrochim. Acta* **1966**, *22A*, 1981.

Table 4. Resonance Raman Frequencies, Intensities and Distortions[a]

frequency	rel intens 647.1 nm	distortion 647.1 nm	rel intens 363.8 nm	distortion 363.8 nm	rel intens 457.9 nm	distortion 457.9 nm
211	<0.01		<0.01		0.05	1.69
236	<0.01		<0.01		0.06	1.55
253	0.10	1.50	<0.01		0.03	1.12
325	0.10	1.19	0.02	1.04	0.02	0.60
361	0.25	1.70	0.06	1.82	0.06	1.05
382	0.22	1.49	0.03	1.10	0.04	0.81
454	0.09	0.79	0.02	0.88	0.03	0.60
463	0.15	1.02	<0.01		0.05	0.76
590	0.51	1.45	0.11	1.45	0.07	0.71
598	0.73	1.71	<0.01		0.11	0.87
690	0.02	0.24	<0.01		0.00	0.12
804	0.01	0.16	<0.01		0.00	0.11
850	0.10	0.46	0.05	0.68	0.02	0.27
866	0.05	0.31	<0.01		0.01	0.20
980	<0.01		0.05	0.56	0.04	0.32
1037	<0.01		0.09	0.74	0.08	0.42
1058	0.07	0.30	0.09	0.74	0.14	0.54
1069	0.05	0.24	<0.01		0.05	0.33
1143	<0.01		0.05	0.48	0.09	0.41
1202	<0.01		<0.01		0.09	0.38
1213	0.20	0.45	0.09	0.65	0.11	0.42
1348	<0.01		0.27	0.98	0.18	0.49
1376	<0.01		<0.01		0.17	0.46
1385	0.27	0.46	0.30	1.02	0.20	0.50
1452	1.00	0.84	1.00	1.77	1.00	1.07
1542	0.13	0.28	0.20	0.75	0.15	0.39
1549	0.07	0.20	0.29	0.90	0.09	0.30

[a] Distortions greater than 0.2 with 457.9 nm excitation or bands observed with 647.1 and 363.8 nm excitation were included in the table. The 647.1 and 363.8 nm distortions were used to calculate the dd and CT absorption bands, respectively.

between these interaction constants is changed, contrary to the results of others.[38−40] In order to obtain the best agreement between the calculated and observed vibrational frequencies, the initial set of force constants was varied. The most important changes were made on the diagonal force constants f_{NN} and f_{BN}, which were increased by 17% and 8%, respectively. In the refinement process, the value of f_{CuN} was decreased by 10% compared to that currently proposed for polyamine complexes.[32,33] Force constants and nondiagonal terms related to the pyrazolyl groups and to the $C-CH_3$ moiety were modified by no more than 5%. In general, the final values used in the calculation have reasonable values. For instance the values for the stretching constants in the skeletal framework and pyrazolyl ring are expected to fall between 4 and 6.5 mdyn/Å, while those ones corresponding to ring bending fall in the range of 1.1−1.7 mdyn Å/rad^2. The final force constants are collected in Table 2.

The frequencies calculated from this set of final force constants are listed in Table 3 along with the calculated potential energy distribution (PED). For the A_1 species, we have included the observed resonance enhanced frequencies for comparison. Results shown in Table 2 indicate, in general, a high degree of mixing among the different vibrational modes. The ν(CuN) is calculated in the range 158−360 cm^{-1}, with different degrees of mixing, δ(NBN) contributes to the band at 325 cm^{-1}, and ν(BN) is calculated at about 700 cm^{-1}. The normal modes to which ν(NN), ν(NC), and ν(CC) primarily contribute are calculated at 1546, 1451, 1380, 1351, and 1218 cm^{-1}.

2. Distortions from Resonance Raman Intensities. The determination of excited state distortions from resonance Raman intensities is a method that has been applied to a wide variety of molecules with different types of electronic transitions.[7−18] Detailed descriptions of the method have been presented in the literature;[7−11] only a brief discussion of the relevant theory and equations are given here. Relative bond distortions are determined from the relative resonance Raman intensities using Savin's formula[8,41]

$$\frac{I_k}{I_{k'}} = \left(\frac{\Delta_k \omega_k}{\Delta_{k'} \omega_{k'}}\right)^2 \quad (1)$$

where I_k is the resonance Raman intensity, Δ_k is the dimensionless bond distortion and ω_k is the vibrational frequency of the k'th normal mode. The relative dimensionless distortions are converted into absolute dimensionless distortions using the absorption spectrum[9]

$$2\sigma^2 = \sum_k \Delta_k^2 \omega_k^2 = \frac{(\mathrm{FWHM})^2}{4 \ln 2} \quad (2)$$

where $2\sigma^2$ is the full width of the absorption spectrum at $1/e$ of its height.

The resonance Raman derived dimensionless distortions can be used to calculate the experimental absorption bands. The absorption bands are calculated with the time-dependent theory of absorption spectroscopy.[9,42] The overlap of a propagating wave packet with the initial wave packet on a multidimensional excited state potential energy surface provides insight into the absorption spectrum in the frequency domain. The overlap has a closed formula expression if the potential surfaces are harmonic, the force constants are the same in the ground and excited states, the transition dipole moment is constant, and the normal coordinates are not mixed in the excited state. The small errors introduced by these approximations are discussed in ref 9. The overlap is given by

(40) Neto, N.; Muniz-Miranda, M.; Angeloni, L.; Castellucci, E. *Spectrochim. Acta* **1983**, *39A*, 97.
(41) Warshel, A.; Dauber, P. *J. Chem. Phys.* **1977**, *66*, 5477.
(42) Heller, E. J. *Acc. Chem. Res.* **1981**, *14*, 368.

$$\langle\phi|\phi(t)\rangle = \exp\left\{\sum_k\left[-\frac{\Delta_k^2}{2}(1-\exp(-i\omega_k t)) - \frac{i\omega_k t}{2}\right] - iE_{00}t - \Gamma^2 t^2\right\} \quad (3)$$

where Δ_k is the dimensionless displacement of the k'th normal mode, ω_k is the vibrational frequency of the k'th normal mode, E_{00} is the energy separation between the lowest vibrational levels of the two states, and Γ is a damping factor. The absorption spectrum in the frequency domain is the Fourier transform of the overlap in the time domain and is given by

$$I(\omega) = C\omega\int_{-\infty}^{\infty} e^{i\omega t}\langle\phi|\phi(t)\rangle\, dt \quad (4)$$

where C is a constant and $I(\omega)$ is the intensity in photons per unit volume per unit time at frequency ω. The dimensionless distortions and vibrational frequencies in Table 4 were used to calculate the experimental absorption bands. The values of E_{00} were determined from the experimental absorption spectrum and were 11 000 cm^{-1} for the ligand field state and 23 500 cm^{-1} for the LMCT state. The value of Γ used in the calculation was 10 cm^{-1}.

The largest intensities in resonance Raman spectra are usually totally symmetric vibrational modes. Therefore in the C_{3v} model, only A_1 modes are expected to be strongly resonance enhanced. The excited state potential energy surface is displaced along the normal coordinate relative to the ground state surface for the A_1 modes. The resonance Raman intensity is proportional to the slope of the excited state potential energy surface. There is thus a close correspondence between the resonantly enhanced vibrational modes and calculated A_1 modes from the normal coordinate analysis.

In the absence of a normal coordinate analysis, the dimensionless distortions are often assumed to involve only one internal coordinate. However, the potential energy distribution shows that the normal modes involve motions of multiple internal coordinates. There is no single motion corresponding to one normal mode. For example, the 361 cm^{-1} normal mode ($\Delta_{red} = 1.70$ and $\Delta_{UV} = 1.82$) consists of 37% δ(NBN), 26% ν(CuN), and 37% $\delta(NCC)_a$. Assigning this mode as a pure Cu−N stretch would exceed that calculated using the PED by 75% because the contributions of the δ(NBN) and $\delta(NCC)_a$ internal coordinates to the normal mode would be neglected.

The distortions can aid in the assignments of the electronic states. The high frequency normal modes between 1200 and 1600 cm^{-1} consist of a mixture of pyrazolyl ring modes. For example, the 1542 cm^{-1} normal mode is a mixture of the $\nu(CC)_a$, $\nu(CC)_b$, $\nu(NC)_a$, $\delta(NCC)_a$, and δ(CCH) local modes, but these motions all arise from the pyrazolyl ring. The distortion of the 1542 cm^{-1} mode changes from 0.84 in the ligand field state to 1.77 in the LMCT state. The larger distortion of this mode in the charge transfer state supports the assignment of the 32 900 cm^{-1} absorption band as a LMCT from the Tp* ligand to the Cu(II) ion. Similar trends are seen in the other high frequency pyrazolyl ring modes.

The dimensionless bond distortions are converted into distortions in Angstroms using the potential energy distribution from the normal coordinate analysis. The equation used to convert the dimensionless distortions, Δ, into distortions in Å, δ, is[14]

$$\delta = 4.43\times10^{-3}\sum_k(\pm)_{ik}\left(\frac{f_{ik}\omega_k}{F_{ii}}\right)^{1/2}(\pm\Delta_k) \quad (5)$$

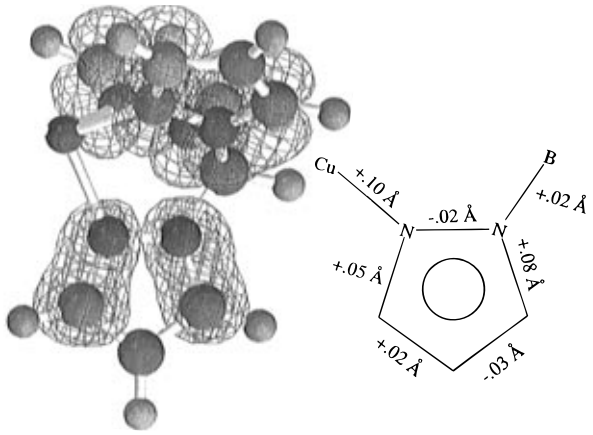

Figure 3. Probability contours for the highest occupied π* orbital of the pyrazolyl group on $Cu(Tp^*)_2$ (left) and the calculated excited state distortions for $Cu(Tp^*)_2$ in the LMCT excited state (right). The perspective is chosen to emphasize the contours on one of the three equivalent pyrazolyl rings in the C_{3v} model.

where δ is the distortion in Å, f_{ik} is the percentage of the normal mode from the PED, ω_k is the frequency in cm^{-1}, F_{ii} is the diagonal force constant, and Δ_k is the distortion of the k'th normal mode. The signs of the internal coordinate changes, $(\pm)_{ik}$, come from the $\boldsymbol{L}$ matrix which transforms the normal coordinates, Q, into internal coordinates, R.

$$R = \boldsymbol{L}Q \quad (6)$$

Unfortunately, the signs of the distortions cannot be calculated because the resonance Raman intensity is proportional to the square of the dimensionless distortion. The directions of the geometry changes along the normal coordinates must be determined by some other method. A restricted Hartree−Fock molecular orbital calculation using a STO-3G basis set was performed to help determine the sign changes of the distortions. (Because the focus is on the CC, CN, and NN bonds of the Tp* ligand, a simplified model was used. The crystalographically determined atomic positions of one Tp*−Cu unit were used, but the remainder of the complex was approximated by three CH_3 groups. The positions of the nodes on the five-membered rings were insensitive to the approximations involving the other ligands on the copper.) The sign changes resulting from removing an electron out of the highest occupied π* orbital on the Tp* ligand were rationalized by inspection of the calculated probability contours which are shown in Figure 3 (left). Removing an electron from an orbital that has bonding character between two nuclei should result in a longer bond length (positive distortion) while a shorter bond length (negative distortions) should occur when an electron is moved from an orbital that has antibonding character between two nuclei. Where the electron density is small between two nuclei, only small changes are expected. Therefore, the $(NC)_a$ and $(NC)_b$ bonds should lengthen, the (NN) bond should shorten, and the $(CC)_a$ and $(CC)_b$ bonds should have small changes. Bond distortions in Å using all of the possible 2^5 sign permutations for the dimensionless distortions of the high frequency 1213−1542 cm^{-1} modes that contain primarily internal coordinates from the pyrazole ring were calculated. The bond length changes for the four permutations with the most reasonable sign changes (based on the nodal pattern from the MO calculation) are given in Table 5. The permutation (−, +, +, +, +) = ($-\Delta_{1542}$, $+\Delta_{1452}$, $+\Delta_{1385}$, $+\Delta_{1348}$, $+\Delta_{1213}$) gives the most reasonable bond length changes because there are no calculated δ's ≥ 0.1 Å. The permutation (+, +, +, +, +) is included in Table 5 because often the distortions are assumed to all have

Table 5. Bond Distortions (δ) in Angstroms as a Function of the Signs of the Distortions of the Normal Coordinates (Δ)

signs[a]	$(NC)_a$	$(NC)_b$	$(CC)_a$	$(CC)_b$	(NN)
		LMCT State			
(−,+,+,+,+)	+0.08	+0.05	−0.03	+0.02	−0.02
(−,+,+,+,−)	+0.10	+0.08	−0.03	+0.02	−0.08
(−,+,+,−,+)	+0.08	+0.10	−0.03	+0.02	−0.02
(−,+,+,−,−)	+0.10	+0.12	−0.03	+0.02	−0.08
(+,+,+,+,+)	+0.03	+0.05	−0.08	+0.07	−0.02
		Ligand Field State			
(−,+,+,+,+)	+0.02	+0.03	−0.02	+0.01	0.00
(−,+,+,+,−)	+0.03	+0.05	−0.02	+0.01	−0.05
(−,+,+,−,+)	+0.02	+0.03	−0.02	+0.01	0.00
(−,+,+,−,−)	+0.03	+0.05	−0.02	+0.01	−0.05
(+,+,+,+,+)	0.00	+0.03	−0.03	+0.03	0.00

[a] The sign combinations are for the 1542, 1452, 1385, 1348, and 1213 cm^{-1} distortions, respectively. $(-, +, +, +, +) = (-\Delta_{1542}, +\Delta_{1452}, +\Delta_{1385}, +\Delta_{1348}, +\Delta_{1213})$.

Scheme 1

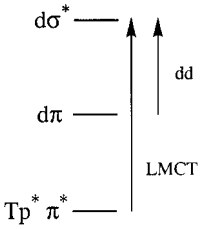

positive signs. However this all positive permutation predicts large changes in the $(CC)_a$ and $(CC)_b$ bonds while the highest occupied π^* orbital shows that they have little electron density between their nuclei and should have small changes. A diagram summarizing the bond length changes in the LMCT excited state is given in Figure 3 (right).

3. Meaning and Analysis of the Distortions. The distortions are measured from the resonance Raman intensities[43−46] for two different excited states. The first state involves a ligand field transition on the Cu(II) ion observed in the red, while the second state is a ligand-to-metal charge transfer from the Tp* ligand to the Cu(II) ion and is in the UV.[47] The electronic transitions for $Cu(Tp^*)_2$ are shown in Scheme 1. The distortions are analyzed in terms of the individual electronic transitions.

In the ligand field state, an electron is promoted from a dπ bonding orbital to a dσ^*orbital. A large distortion in the Cu−N bond is expected since the transition is centered on the d orbitals of the Cu(II) ion. However, within the rigid framework of the Tp* ligand other bonds must also distort as a result of the Cu−N bond lengthening. The largest change is observed in the $(NC)_b$ which is near the copper. However these distortions are an upper limit because the observed resonance Raman scattering intensity might have contributions from nonresonant terms since the oscillator strength for the ligand field state is small.

In the LMCT state, an electron is taken out of the π^* orbital on the Tp* ligand and excited to a dσ^* on the Cu(II) ion. Large distortions on the Tp* ligand are expected since an electron is taken out of a bonding molecular orbital. Surprisingly, the distortion in the Cu−N bond is larger than that in the ligand field state. The excited electron enters the same orbital in both transitions, however in addition there is a charge effect in the LMCT state. In the LMCT excited state, the Cu−N bond distance should be longer because the copper is formally reduced and the Cu(I)−N distance is greater than the Cu(II)−N distance. Both a charge effect and the population of an antibonding orbital occur in the LMCT state whereas only the population of an antibonding orbital occurs in the ligand field state.

Calculation of metal-ligand bond length changes in excited electronic states have been the subject of many papers.[18,43−46] Specifically Cu(II) complexes including those containing Cu−N bonds have been reported. Bond length changes range from 0.07 to 0.25 Å.[44] Our values of 0.067 Å in the ligand field and 0.10 Å in the LMCT state are typical for copper complexes. The observed Cu−N bond length changes are also consistent with those measured in the blue copper protein plastocyanin.[11]

Calculated excited-state bond length changes in ring systems are rare. In a study of pyridine coordinated to an iron porphyrin, C═C and C═N changes between 0.010 and 0.016 Å were calculated.[12] In a study of uracil, a C═C change of 0.14 Å was observed.[14,15] The changes that we calculate are within the previously reported ranges.

In both the ligand field and LMCT states the entire framework of the Tp* ligand is distorted. In the three skeletal six-membered rings made up of copper, four nitrogens, and the boron atoms, all of the bond lengths and angles change. It is interesting to note that the B−N tripod angle increases even though the σ orbitals are not primarily involved in the transition. The calculated angle change of −2° is a result of both the Cu−N lengthening which pushes the entire framework outward and the mixing of δ(NBN) and ν(CuN) as shown in the PED. This complex is an interesting case where metal ligand vibrations cannot be treated as uncoupled from the skeletal motions in the molecule.

Summary

We report a normal coordinate analysis of $Cu(Tp^*)_2$ and obtain a good fit to the experimental frequencies. A normal coordinate analysis is necessary in order to obtain bond length changes in the cagelike molecule because the internal coordinates are highly mixed. Resonance Raman intensities are useful in the normal coordinate analysis to help assign the totally symmetric modes. The intensities are also used to calculate the excited state distortions. The signs of the bond length changes are consistent with those expected from the nodal pattern from a molecular orbital calculation.

Acknowledgment. This work was supported by the National Science Foundation Grant CHE-9509275. The authors wish to thank Susan Haldemann for the molecular orbital calculation of $Cu(Tp^*)_2$. GDF and MCV wish to thank FONDECYT Project 1950397. GDF thanks the Universidad de Playa Ancha for research facilities.

IC961006L

(43) Hitchman, M. A. *Inorg. Chem.* **1982**, *21*, 821.
(44) Deeth, R. J.; Hitchman, M. A. *Inorg. Chem.* **1986**, *25*, 1225.
(45) Shin, K. S. K.; Clark, R. J. H.; Zink, J. I. *J. Am. Chem. Soc.* **1989**, *111*, 4244.
(46) Shin, K. S. K.; Clark, R. J. H.; Zink, J. I. *J. Am. Chem. Soc.* **1990**, *112*, 3754.
(47) Murphy, A.; Hathaway, B. J.; King, T. J. *J. Chem. Soc. Dalton Trans.* **1979**, 1646.